Supplemental material to:

Direct evidence of Be as an amphoteric dopant in GaN

U. Wahl, J.G. Correia, A.R.G. Costa, T.A.L. Lima, J. Moens, M.J. Kappers, M.R. da Silva, A. Vantomme, and L.M.C. Pereira

Note: numbers of references are with respect to those in the main paper

1. Details on GaN samples used

Sample	nid-GaN #2	nid-GaN #3	nid-GaN #1	*p*-GaN:Mg	*n*-GaN:Si
Internal number	#398	#468 (SLA64 LA23)	#501	#491	#488
Year of growth/purchase	<2010	<2011	2014	2014	2014
Growth method	MOCVD	HVPE	MOCVD	MOCVD	MOCVD
Grower	IMEC	Kymatech	U Cambridge	U Cambridge	U Cambridge
Dopant concentration	undoped	undoped	undoped	2×10^{19} cm^{-3}	1×10^{19} cm^{-3}
Doped layer thickness [nm]	-	-	-	150	150
Film thickness [µm]	not known	5	4.8	4.8	4.8
Substrate	sapphire	sapphire	sapphire	sapphire	sapphire
Mosaic W_{tilt}		0.077°	0.07° [a)]	0.07° [a)]	0.07° [a)]
Mosaic W_{twist}		0.182°	0.08° [a)]	0.08° [a)]	0.08° [a)]

MOCVD = Metal Organic Chemical Vapor Deposition
HVPE = Hydride Vapor Phase Epitaxy
[a)] typical values, M. Kappers, private communication

2. Schematic illustration of the emission channeling technique

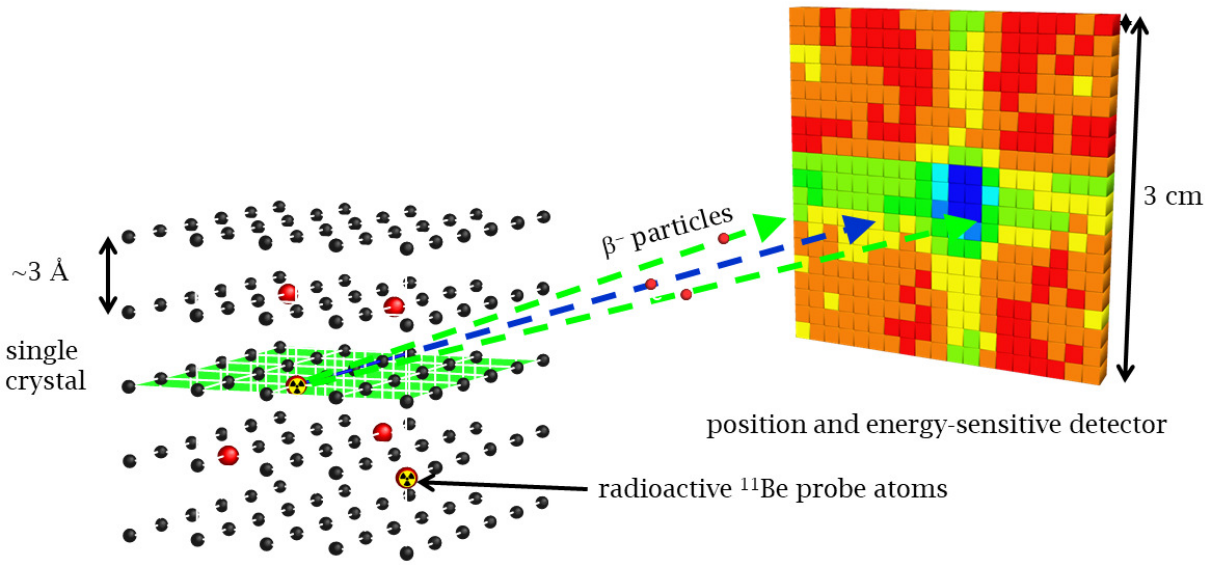

FIG. S1. Schematic illustration of the emission channeling method. Radioactive ^{11}Be ($t_{1/2}$=13.8 s) probe atoms are implanted into GaN single crystalline films. A position-sensitive detector is used to detect emitted β^- particles in the vicinity of major crystallographic directions. Depending on the lattice site of the ^{11}Be atoms, emitted β^- particles are channeled or blocked on their way out of the crystal. In this example, axial channeling is indicated by the blue arrow and the blue, enhanced yield in the center of the detector, while planar channeling is indicated by green arrows and green, enhanced yields.

3. Position of interstitial Be_i in the GaN wurtzite lattice in comparison to Mg_i

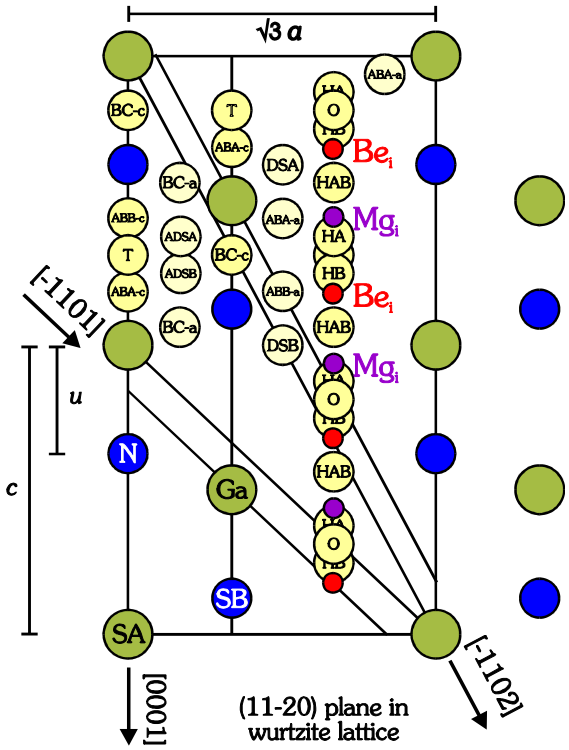

FIG. S2. (11−20) plane in the GaN wurtzite lattice, showing the Ga (SA) and N (SB) atom positions and the major interstitial sites (a=3.189 Å, c=5.185 Å, u=0.375 c). The octahedral sites O are located in the wide-open interstitial region parallel to the [0001] axis and exactly centered in between planes of Ga and N atoms, as are the "hexagonal" HAB sites, while HA and HB are interstitial positions that are collinear with the basal Ga-N bond directions and have as closest neighbors A or B atoms, respectively. The **red** circles represent the best fit results for the position of interstitial **Be_i**, which is shifted by +0.693(76) Å from the ideal octahedral O site via the HB towards the HAB sites. In comparison, the corresponding positions for **Mg_i** as identified in Ref. [7] in p-GaN, −0.60(13) Å from the ideal octahedral O site via the HA towards the HAB sites, are indicated by the **purple** circles.

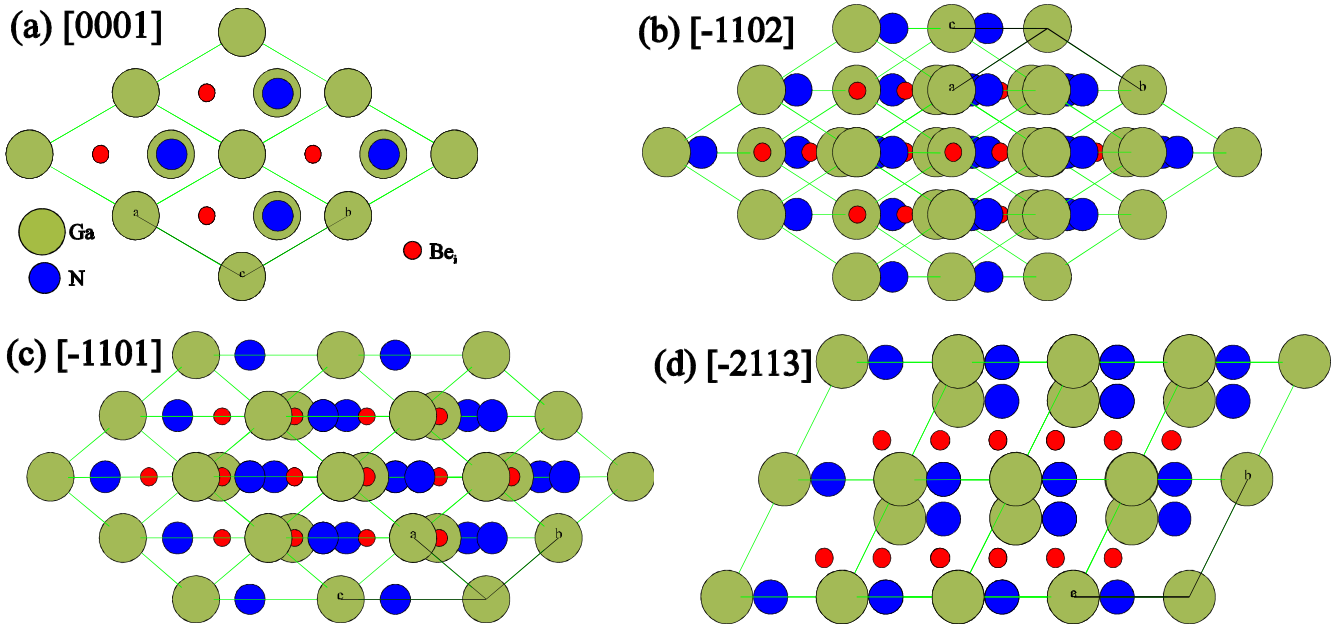

FIG. S3. Projections of the four major axial directions in wurtzite GaN, indicating with red circles the identified positions of interstitial Be_i. Note that along the [0001] and [−2113] directions the projections of both equivalent Be_i positions are fully interstitial, while along [−1102] and [−1101] in each case one of the two projections is approximately aligned with a string of Ga atoms. Correspondingly, electron emission from $^{11}Be_i$ exhibits some channeling effects along [−1102] and [−1101] while along [0001] and [−2113] it shows pronounced minima (cf. Fig. 3 of main paper).

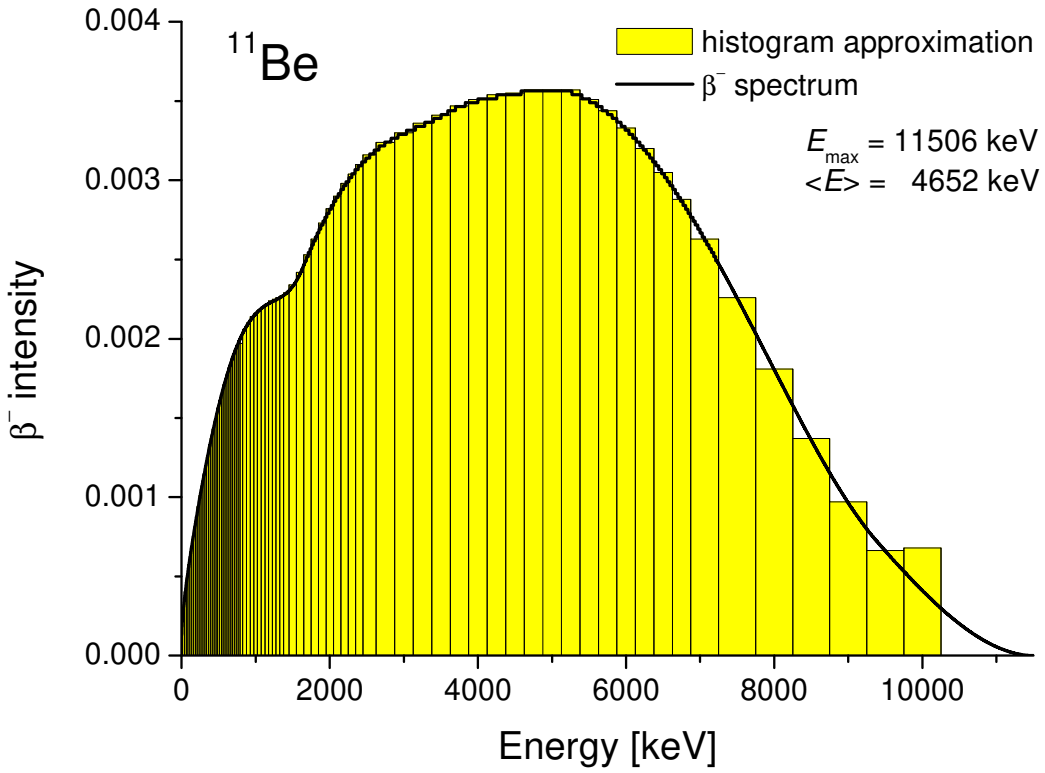

FIG. S4. β^- spectrum of ^{11}Be and the histogram (in yellow) of the energy values used to approximate it in the "many-beam" calculations.

4. Many-beam simulations

In order to quantitatively analyze the experimental electron emission distributions, they were fitted by linear combinations of theoretical emission patterns for various lattice sites, which were calculated using the "many-beam" formalism for electron channeling [34,35]. ^{11}Be decays by the emission of β^- particles with an endpoint energy of 11506 keV (average β^- energy 4652 keV). To account for the continuous β^- spectrum, "many-beam" simulations were performed for a number of discrete electron energies, as are listed in Table S1, and weighted according to the β^- spectrum of ^{11}Be (Fig. S4). Angular patterns were calculated in *x*- and *y*-direction from −3° to +3° in steps of 0.025° for 200-250 different lattice sites in the wurtzite structure. The designations and positions of the major sites of highest symmetry are shown in Fig. S1. The patterns resulting from the occupancy of SA, SB, T, ABA(c), O, HA, HB, HAB, BC(c), ABB(c), BC(a), and ABA(a) sites are shown in Figs. S6-S8.

Energy range [keV]	Energy step width [keV]	
25-800	25	
800-1400	50	
1400-2500	100	
2500-7000	250	
7000-10000	500	

Table S1. Step width of energies used in the many-beam electron channeling simulations

Energy range [keV]	Number of "beams" n	Number of Fourier components of continuum potential $(2n+1)^2$	Number of Fourier components of electron wave functions $(n+1)^2$
25-100	20	1681	441
125-1700	24	2401	625
1800-3000	28	3249	841
3250-5500	32	4225	1089
5750-6250	36	5329	1369
6500-9000	40	6561	1681
9500-10000	44	7921	2025

Table S2. Number of "beams" and corresponding numbers of Fourier components used in the many-beam electron channeling simulations.

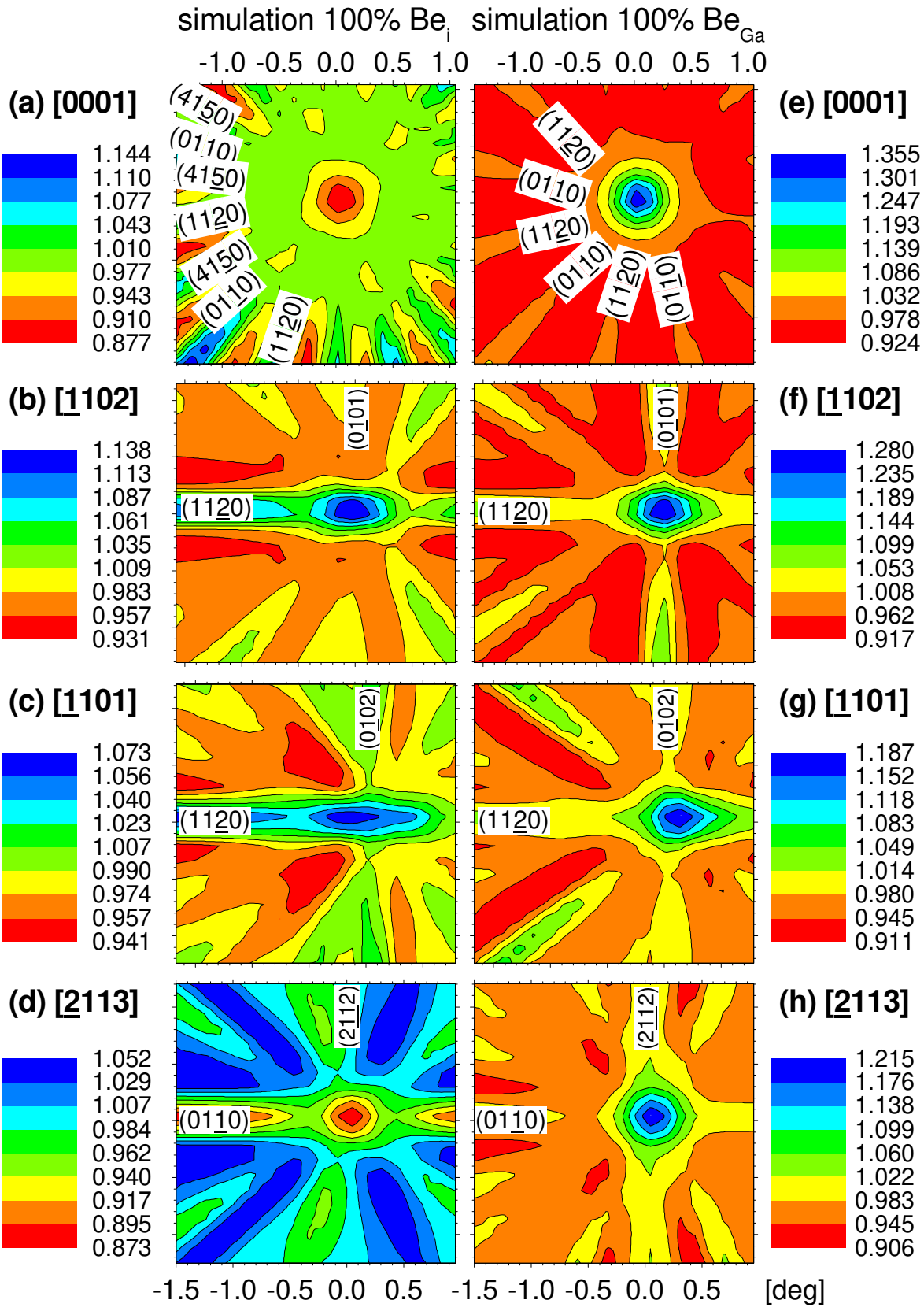

FIG. S5. Simulated β^- emission channeling patterns for 30 keV implanted ^{11}Be in GaN along the four major crystallographic directions. (a)-(d) are patterns for 100% of emitter atoms on the Be_i interstitial sites, i.e. shifted by +0.69 Å from ideal O sites via HB towards the HAB position, while (e)-(h) are for 100% on substitutional Ga sites Be_{Ga}. The orientation of all patterns has been chosen so as to correspond to the RT measurements of the *p*-GaN:Mg sample as shown in Fig. 1(a)-(d) of the main paper. Note that this figure is identical to Fig. 3 of the main paper but with the most prominent major planes indicated.

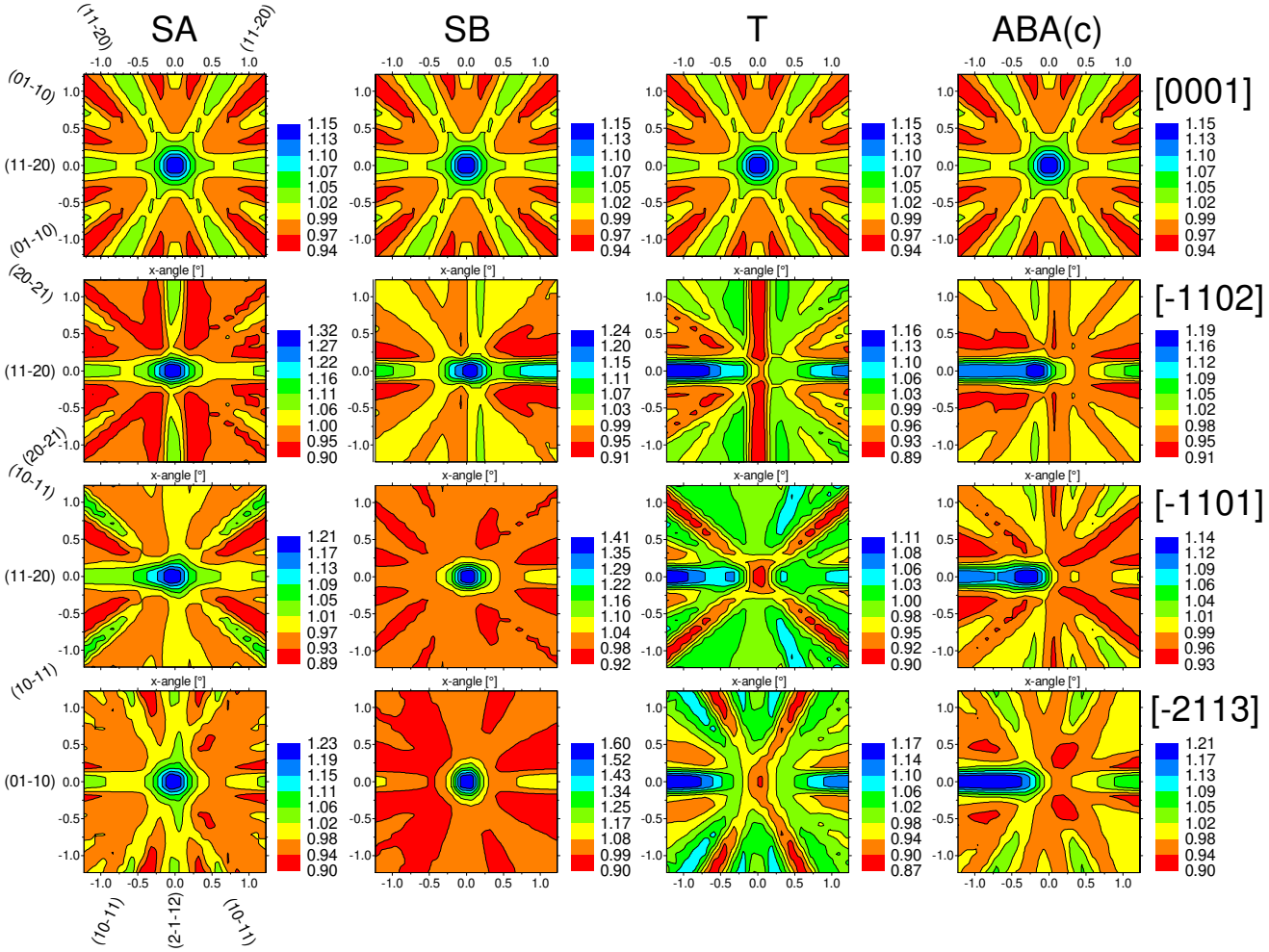

FIG. S6. Theoretical β^- emission patterns from ^{11}Be on substitutional Ga (SA), substitutional N (SB), tetrahedral interstitial T and ABA(c) sites around the [0001], [−1102], [−1101], and [−2113] axes of GaN. Note that all of these sites are aligned with the *c*-axis atomic rows, so their [0001] patterns are all identical.

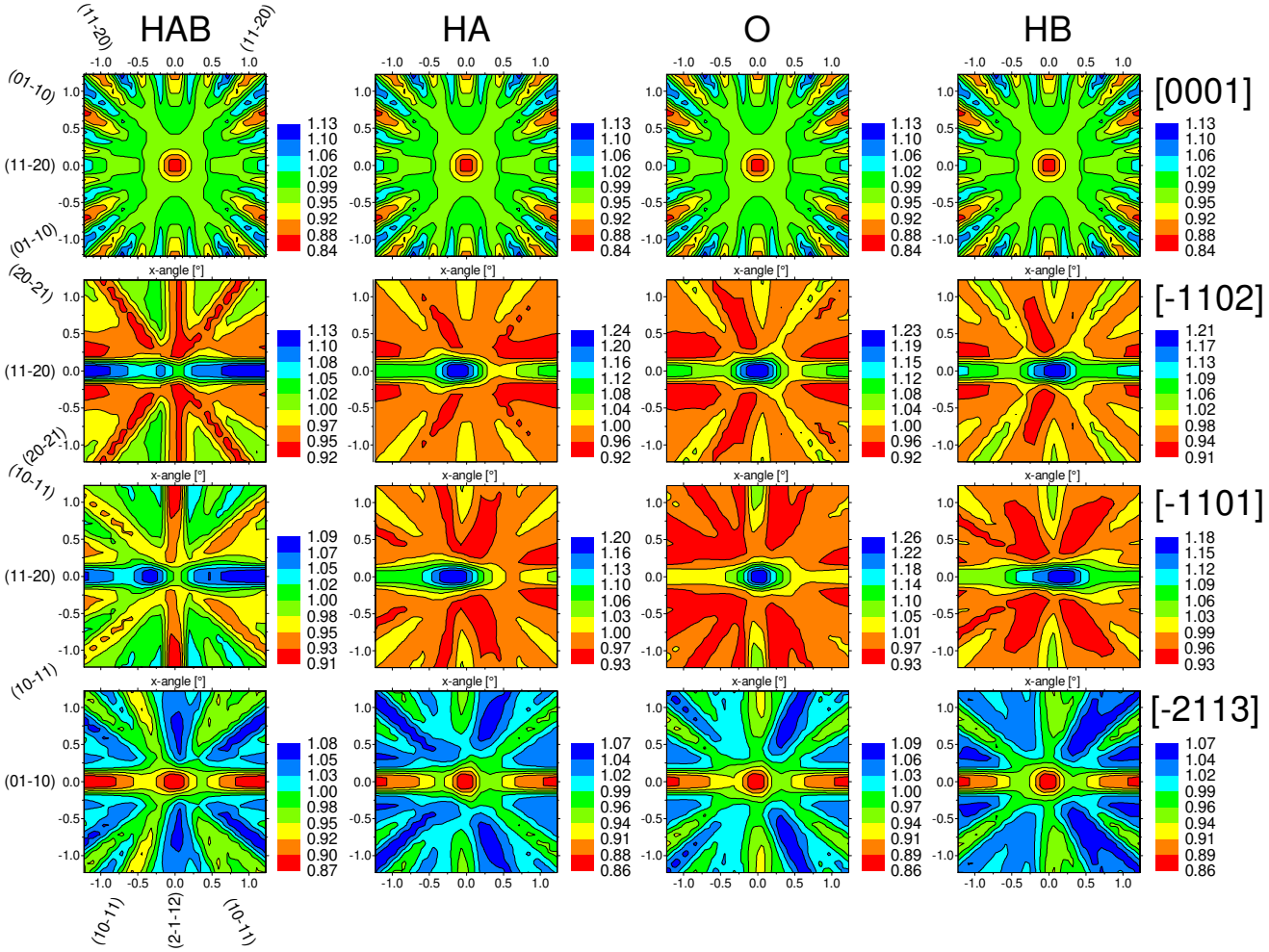

FIG. S7. Theoretical β^- emission patterns from ^{11}Be on interstitial HAB, HB, O and HA sites around the [0001], [−1102], [−1101], and [−2113] axes of GaN. Note that with respect to the *c*-axis, all of these sites are located in the center of the wide-open interstitial region parallel to the *c*-axis, so their [0001] patterns are all identical.

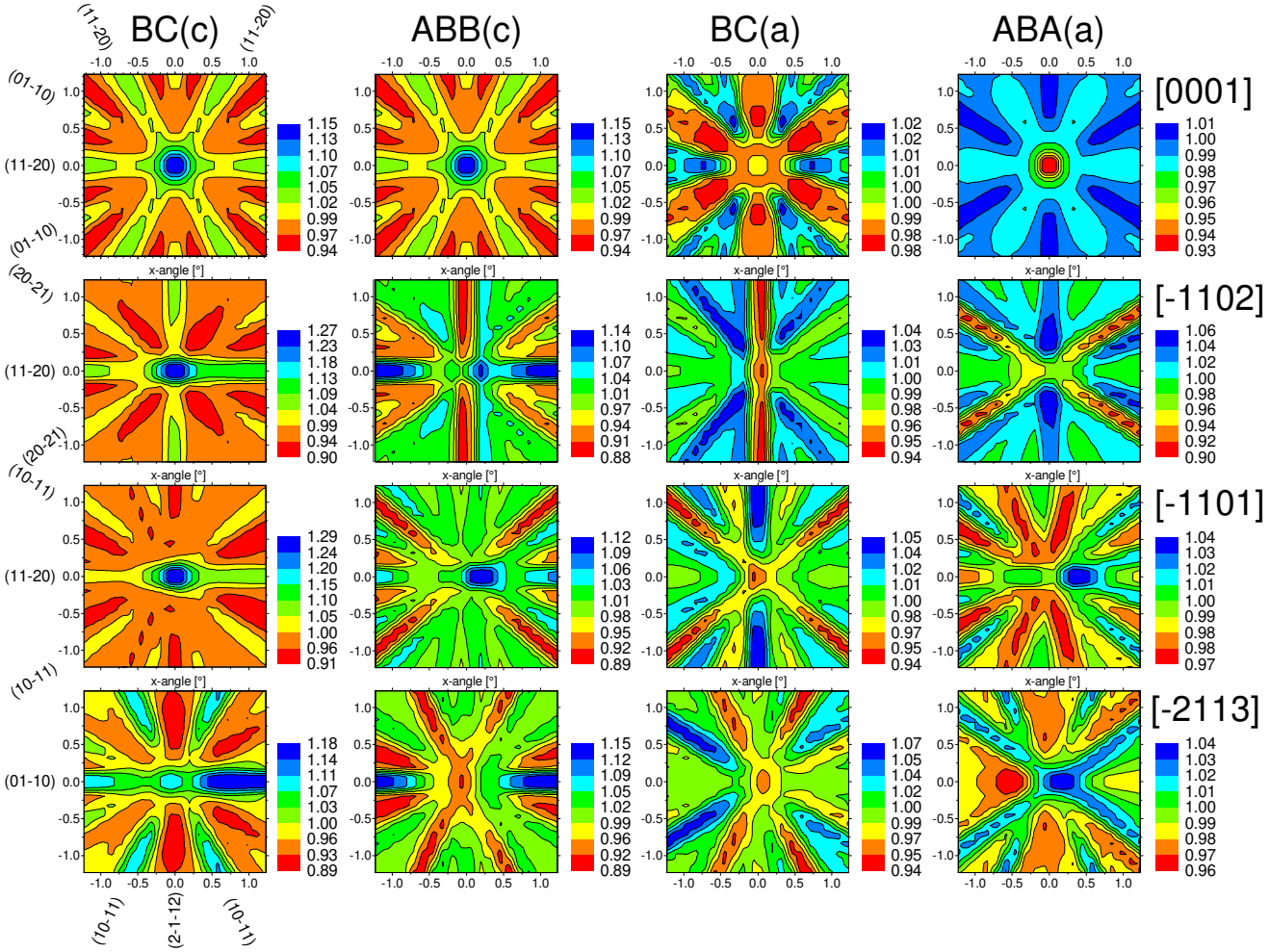

FIG. S8. Theoretical β^- emission patterns from ^{11}Be on BC(c), ABB(c), BC(a) and ABA(a) sites around the [0001], [−1102], [−1101], and [−2113] axes of GaN.

5. Channeling patterns from nid-GaN samples #1 and #3

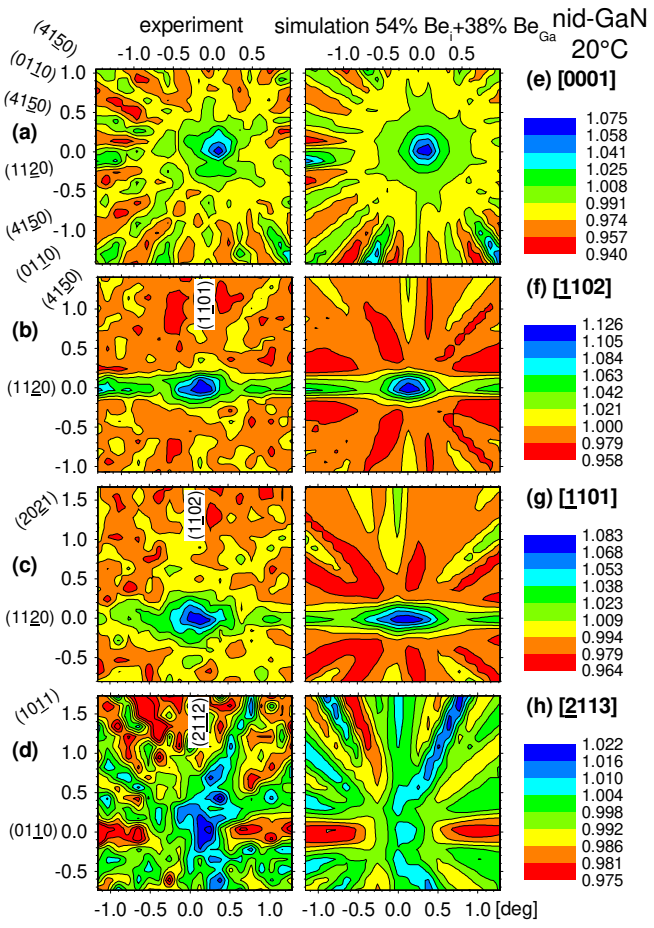

FIG. S9. (a)-(d) Angular distribution of β⁻ emission yields from ^{11}Be in nid-GaN #3, measured during RT implantation. (e)-(h) are the best fits of simulated patterns, corresponding to 54% on Be$_i$ interstitial and 38% on Be$_{Ga}$ sites. The major planar directions are indicated. Number of events per pattern: (a) 3.7×10^6, (b) 3.3 ×10^6, (c) 2.3 ×10^6, (d) 7.0 ×10^6.

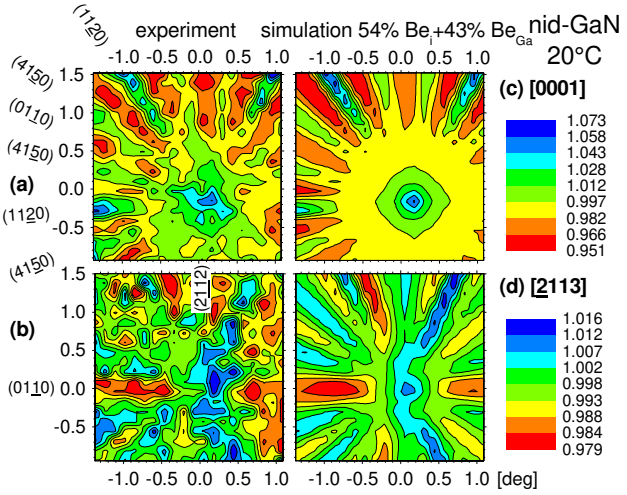

FIG. S10. (a)-(b) Angular distribution of β⁻ emission yields from ^{11}Be in nid-GaN #1, measured during RT implantation. (c)-(d) are the best fits of simulated patterns, corresponding to 54% on Be$_i$ interstitial and 43% on Be$_{Ga}$ sites. The major planar directions are indicated. Number of events per pattern: (a) 3.3×10^6, (b) 6.4 ×10^6.

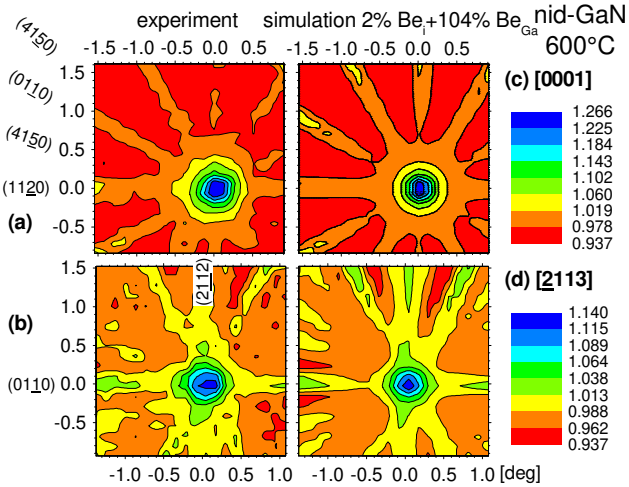

FIG. S11. (a)-(b) Angular distribution of β⁻ emission yields from ^{11}Be in nid-GaN #1, measured during 600°C implantation. (c)-(d) are the best fits of simulated patterns, corresponding to 2% on Be$_i$ interstitial and 104% on Be$_{Ga}$ sites. The major planar directions are indicated. Number of events per pattern: (a) 7.1×10^6, (b) 5.1 ×10^6.

6. Background correction factors

Measurements of electron emission channeling effects are always subject to background which arises from two sources. First there is the contribution from electrons that are backscattered from inside the sample or from the walls of the vacuum chamber. This effect can only be theoretically estimated, in our case by performing GEANT4 Monte Carlo simulations of electron trajectories. It is estimated that 42% of the total electron count rate results from backscattered electrons, which amounts to a correction factor of 1.7 for the fitted fractions.

The second contribution arises from the background of gammas that are either emitted by the sample itself, by radioisotopes in the vicinity, or which result from cosmic radiation. The gamma background can be experimentally estimated by closing a shutter valve in front of the detector, which stops all electrons from the sample but allows most of the γ particles to pass. While routinely performed at intervals during the experiments, this procedure does not allow to continuously monitor the background. The gamma background in *off-line* experiments with long-lived radioisotopes is generally rather stable with time, however, in *on-line* experiments with short-lived isotopes such as ^{11}Be it is subject to fluctuations. These arise basically from two sources. First of all, the collimation of the ISOLDE beam to 1 mm diameter by means of a nozzle results in only about 50% of the ^{11}Be beam being implanted into the sample. The rest is deposited inside the collimating nozzle, which is located about 25 cm from the sample (cf. Ref. [43] for a sketch of the experimental setup). The gamma radiation emitted by the ^{11}Be isotopes deposited in the nozzle, while shielded from direct line of sight towards the detector, partially passes through the shielding and thus also contributes to the detector count rate. If the focusing of the ion beam changes, so do the relative contributions of ions implanted into the sample and deposited inside the collimating nozzle, which somewhat changes the signal to background ratio. A second source of gamma background is the overall gamma background in the ISOLDE experimental hall and in the vicinity of the detector. In the case of ^{11}Be experiments this source of background is particularly relevant. ^{11}Be is produced by spallation reactions when bombarding UC_2 targets by a 1.4 GeV proton beam. By means of spallation or fission, the proton beam also produces various radioactive noble gas isotopes, e.g. of Rn or Xe [45]. These can diffuse out of the target material and, while not being ionized, migrate through beam lines in atomic form. Since the beamline valves in case of the short-lived ^{11}Be (13.8 s) have to remain open all of the time, noble gas isotopes also reach the vicinity of the detector, where they contribute to the gamma background, before being extracted by the vacuum pumps. This source of background is absent for experiments with longer lived isotopes, where the beam line valves can be kept closed during the measurements, or much less pronounced for isotopes which are produced from lighter and non-fissile target materials (e.g. ^{27}Mg from Ti targets). On the other hand, in experiments with short-lived isotopes such as ^{11}Be, gamma background from cosmic radiation is usually negligible in comparison to the high electron count rate from the sample.

If derived sum fractions $f_{sum}=f_i+f_S$ somewhat higher than 100% are obtained, this indicates that the background that is contributed by scattered electrons and was simulated by means of GEANT4, has been systematically overestimated to some extent (the expected accuracy of the scattered electron background simulations is of the order of ±10%. Gamma particles contributed in most cases with around 15% to the count rate, but overall fluctuations ±5-10% are common, and thus may lead to similar fluctuations in the estimated sum fractions $f_{sum}=f_i+f_S$. Note that both sources of background, scattered electron and gamma, do not affect the relative fractions, e.g. f_i / f_i+f_S.